Silicon (2023) 15:2745–2752
https://doi.org/10.1007/s12633-022-02219-z

ORIGINAL PAPER

Morphological, Optical, and Crystalline Analysis of $ZnTiO_3$ Nanostructures Deposited on Porous Silicon Substrate

Marouan Khalifa[1] · Hammedi Khadija[1,2] · Chaker Bouzidi[3] · Hatem Ezzaouia[1]

Received: 8 September 2022 / Accepted: 4 November 2022 / Published online: 9 November 2022

Abstract
Zinc titanate ($ZnTiO_3$) was grown on silicon and porous silicon. $ZnTiO_3$ layers were prepared by sol-gel method. Porous silicon was fabricated by electrochemical etching of silicon in HF solution. The effect of substrate porosity on morphology, structure and otpical properties of $ZnTiO_3$ nanostructures has been studied. Theses properties were investigated using XRD, Ultraviolet–Visible spectroscopy, and HRTEM. Some important parameters (absorption, reflectivity (R (%) and grain size) were studied. It was found that the Structural, morphology and optical properties of $ZnTiO_3$ layers are dependent strongly on the type of substrates. The crystalline size decreased for $ZnTiO_3$ layers deposited on PS substrate. The average grain size is about 80 nm for $ZnTiO_3$ grown on porous silicon. The surface morphology of films was also found to be uniform and homogeneous. $ZnTiO_3$-PS shows enhancing photon absorption compared to $ZnTiO_3$-Si.

Keywords $ZnTiO_3$ · Porous silicon · UV-Vis · XRD · HRTEM

1 Introductuion

Metal oxide semiconductors have recently shown great influence in the fields of photocatalysis [1–3], optoelectronics [4–6], and solar cells [7]. Amongst the studied semiconductors, Zinc oxide (ZnO) has received much attention. It is a wide-bandgap oxide semiconductor with a direct energy gap of about 3.37 eV. ZnO has high chemical and mechanical stability; furthermore, it is nontoxic and widespread in nature [8, 9]. TiO_2 has also shown promise in the areas of photocatalysis [2], solar cells [10], gas sensor and other optical applications [11, 12]. Enormous increase of applications based on ZnO and TiO_2 has been caused not only by the improvements of their intrinsic properties but also by the achievements of transition metal doping and mixed oxides formations.

So, TiO_2 and ZnO have been used to fabricate ZnO-TiO_2 composite materials, annealing conditions and ZnO/TiO_2 molar ratio were found have significants effects on the phase formation [13]. The coupling TiO_2/ZnO gives a material named zinc titanate that enhances the properties of ZnO and TiO_2, for example, by widening its light absorption spectrum [14]. Additionally, the photocatalytic activity of oxides may help reduce the susceptibility of pollutants to form aggregate structures [15].

However, zinc titanate system has three compounds that exist in the: $ZnTiO_3$, $Zn2Ti_3O_8$, and Zn_2TiO_4, which it remains as a structural defect. $ZnTiO_3$ is a perovskite-type oxide (ABO_3) whose perovskite structure endows the flexibility to alter the arrangement of the A- and B-sites, and incorporates cation combinations at the A- and B-sites to assemble substituted perovskites. ABO_3 have been considered as materials with various applications in solid oxide fuel cell electrodes (SOFC) [16], metal barriers [17], sensors [18], electronics [19] and catalysts [20]. As a well-known member of this family, zinc titanate ($ZnTiO_3$) has been used as pigments [21], dye adsorbents [22], sensors such as NO and CO gases [23], microwave resonator materials [24], heat reflective pigments [25] and Photocatalyst [26].

✉ Marouan Khalifa
khalifa_marouan@yahoo.fr

[1] Laboratoire de Photovoltaïque (LPV), Centre de Recherches et des Technologies de l'Energie (CRTEn), BorjCedria B.P N°952050, Hammam Lif, Tunisia

[2] Faculty of Mathematical, Physical and Natural Sciences of Tunis, University of Tunis El Manar, Tunis, Tunisia

[3] Laboratory of Physico-Chemistry of Mineral Materials and their Applications, National Center for Research in Materials Sciences, Borj Cedria Technopark, BP 73, 8027 Soliman, Tunisia

Several methods are used to synthesize Zinc titanate ($ZnTiO_3$), as solid state reaction [27], Sol-gel [28, 29], Pechini process [30], Hydrothermal method [31], Sputtering [32], Microwave heating [33], and molten salt Method [34]. Zinc titanate ($ZnTiO_3$) thin films deposited on different substrates. The investigation of the influence of various substrates such as Si (100) [35], glass [36], quartz substrate [37], and ITO coated glass [38] has also been studied.

In This work, porous silicon (PS) is another candidate as substrates due to adjustable roughness (large internal surface), high resistance, strong absorbability, and potential for the development of silicon-based optoelectronic devices. Porous silicon has been used to deposit metal oxides and obtain good quality thin layers [39–41]. we report the growth of $ZnTiO_3$ hexagonal and nanoscale on silicon and porous silicon substrates by spin coating. Optical, morphology and crystal structure of hexagonal and nanoscale were studied by UV-Vis, XRD and TEM techniques. The experimental findings on the effect of the sponge- like structure of the porous silicon substrates on the crystallinity properties of the $ZnTiO_3$ thin films are presented and the causes are discussed.

2 Experimental Details

For the fabrication of nanostructures, porous Si (PSi) substrates were obtained by electrochemical etching [40, 41] of p-type, (100) oriented silicon (Si) wafers with a resistivity of 10–20 Ω cm. For the preparation of the porous substrates, c-Si wafers were cleaned with 2-propanol (under sonication) for 4 min. The Si wafers were rinsed with deionized water, dried with N2 flux, and immersed in hydrofluoric acid aqueous solution (2%) for 4 min, followed by rinsing with deionized water and ethanol and dried under N2 flux. The etching process was carried out for 15 min in hydrofluoric acid (HF, 40 wt%) and ethanol (1:1 volumetric ratio) solution at a constant current density of 10 mA/cm2. After the etching process, the substrates were rinsed with ethanol and dried with N2 flux.

On the other hand, $ZnTiO_3$ nanostructured films on PSi and Si substrates were obtained by spin coating deposition. The formation of $ZnTiO_3$ and the corresponding characterization have been widely studied in the literature [28, 29, 35]. Zinc titanate thin films was prepared by the sol-gel method. In general, Zinc acetate dihydrate (Zn (CH3COO)2·2H2O, Sigma Aldrich, reagent grade, 99% purity), and Titanium (IV) n-butoxide (Ti(O(CH2)3CH3)4, Sigma Aldrich, reagent grade, 99% purity) were used as Zn and Ti source materials, respectively. The Zinc acetate and tetrabutyl titanate were dissolved into ethylene glycol monoethyl ether and acid acetic acid solvent at 80 °C and stirred for 30 min to form clear solution.

For the deposition, PSi and Si substrates with a dimension of 20 mm × 20 mm were used. The substrates were washed successively with acetone, hydrochloric acid aqueous solution, deionized water and absolute ethanol in an ultrasound bath. Then, dried at 100 °C for 10 min before coating. ZnTiO3 precursor solution was spin-coated on the sustrates at 3000 rpm during 30 sec. The as-prepared films were annealed at 120 °C for 10 min to remove organic materials and then at 700 °C for 2 hours to crystallize them into a perovskite structure in a rapid thermal annealing furnace. The process from coating to annealing was repeated 2, 4, 6 and 8 times to produce different thickness of the films. The as prepared and sintered samples were subjected to various analyses by suitable analytical technique.

The structural properties of the prepared materials were studied by XRD analysis using (BRUKER D8 advance model, at room temperature). The morphology of $ZnTiO_3$ was analyzed by high resolution transmission microscopy (TEM), using a HRTEM JEOL2100F microscope. UV-vis absorbance and reflectance spectroscopy analysis (UV-vis) was carried out using Perkin Elmer Lamda 950 spectrophotometer.

3 Result and Discussion

3.1 XRD Analysis

The thicknesses of the films resulting of the 2, 4, 6 and 8 repetitions of spin coating and annealing were found to be 80 nm, 120 nm, 160 nm and 240 nm.

To study the effect of substrate (Silicon, Porous silicon) on crystal structure of $ZnTiO_3$, we performed XRD experiments on the samples. The XRD analysis of $ZnTiO_3$/Si and $ZnTiO_3$/PSi were reported as in Fig. 1. The crystal planes (104), (110), (024), (116), (214), for hexagonal $ZnTiO_3$ (JCPDS card No.26–1500) in the diffractograms can be indexed [30, 42, 43].

The (104) peak is more intense in the $ZnTiO_3$/PSi compare to ZnO/Si. The peak (110) peak appeared in the $ZnTiO_3$/PSi compare to ZnO/Si. Consequently, there traduces better crystallinity of $ZnTiO_3$ formed on PSi than on Si. The difference in intensity can be explained by higher absorption rate of the capillary effect presented in $ZnTiO_3$/PSi sample and the high adhesion due to the high specific surface area in the case of PSi.

The average crystallite sizes of the nanoparticles $ZnTiO_3$ can be estimated using Scherrer equation which is defined as $d = (0.94\ k)/(b\cos(\theta))$, where d is the average grain size, k is the X-ray wavelength (0.15406 nm), b is the full-width at half maximum (FWHM), and θ is the diffraction angle (32.9°). The strongest peaks (104) in XRD were used to calculate the grain size for $ZnTiO_3$. Applying Scherrer's

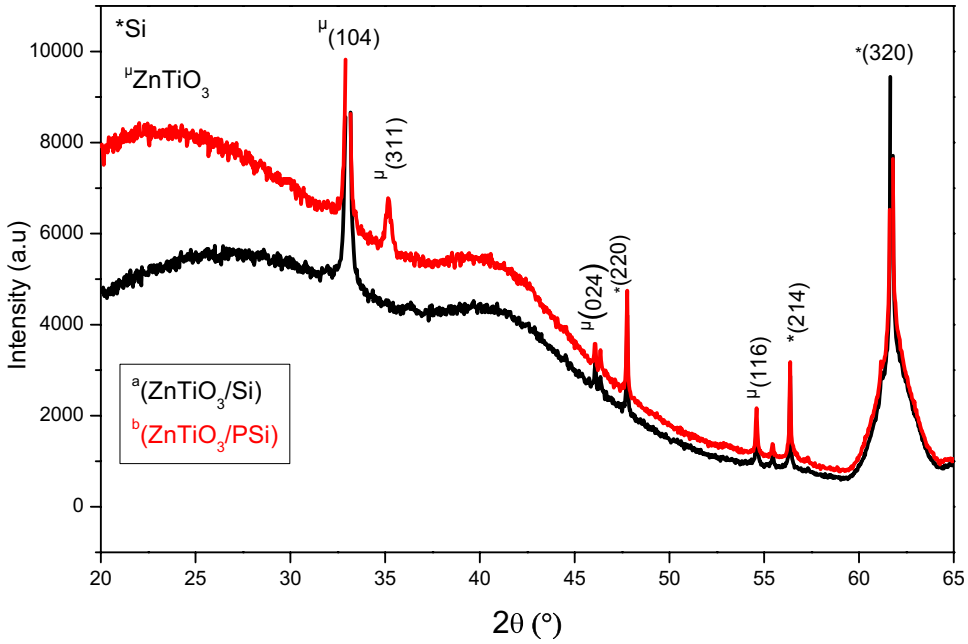

Fig. 1 X-ray diffraction of $ZnTiO_3$ nanostructures grown on conditions on (**a**) Si substrate, (**b**) PSi substrate

formula, the grain sizes were found to be 45 nm and 20 nm for $ZnTiO_3$ formed on PSi and $ZnTiO_3$ formed on Si, respectively. The obtained values indicate that the porous layer has a significant effect on the synthesis mechanism of $ZnTiO_3$ nanostructures and can serve as the starting point for the growth of nanostructures. Therefore, the rough surface morphology of PSi plays a major role in controlling the growth of the wettinglayer [44]. Due to its special surface morphology, the porous layer is a good substrate for lattice-mismatched heteroepitaxy. The surface of the porous silicon layer is composed of many nanocrystals. These Si nanocrystals maintain (100) orientation with the outer surface of the silicon wafer. These randomly distributed Si crystallites on the surface act as nucleation sites and induce the growth of $ZnTiO_3$ nanostructures along the preferred orientation.

3.2 Optical Properties

Optical properties of the $ZnTiO_3$/Si and $ZnTiO_3$/PSi samples have been investigated using UV-Vis spectroscopy. Figure 2 compares the absorbance of $ZnTiO_3$/Si and $ZnTiO_3$/PSi. The layer thickness of $ZnTiO_3$ for two samples is on the order of 120 nm. As shown in Fig. 2, the absorbance recorded in the spectral range 250–900 nm. The spectrum a corresponding to the samples reveals three bands. A first UV absorption band extending from 250 to 270 nm with a sharp band located at about 260 nm, second band with a centered at about 350 nm, and three absorption band extending from 350 to 900 nm.

The band edge is observed at ~280 (first band) and ~400 (second band) nm for all samples. Those bands edge absorption intensity show its absorbance capacity in UV light of

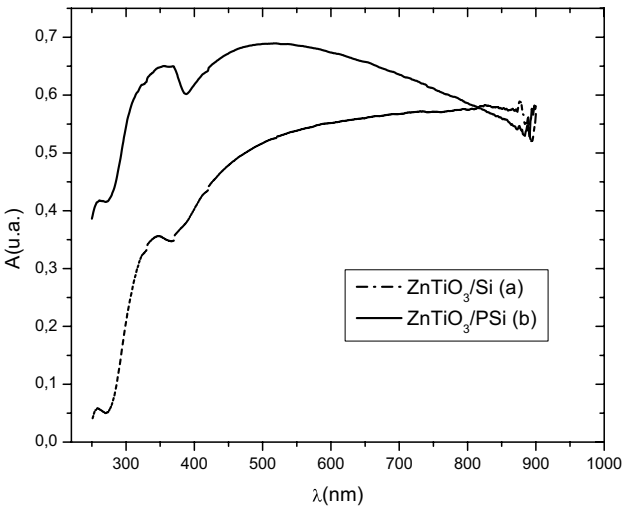

Fig. 2 UV-Vis spectra of $ZnTiO_3$ nanostructures grown on conditions on (**a**) Si substrate, (**b**) PSi substrate

$ZnTiO_3$. it is similar as reported in the literature [45, 46]. The absorbance increases with the porous layer due to the increasing to optical path in porous silicon specific surface. The increase in the visible absorbance (three band) confirmed that the $ZnTiO_3$ nanoparticles are emerged in the pores and therefore are deposited on the specific surface. We deduce that the $ZnTiO_3$/PS acts as an efficient solar absorber.

Optical absorbance spectra of multilayer $ZnTiO_3$ films on porous silicon are shown in Fig. 3. It is seen from this Figure; the spectrum is similar to Fig. 2 with variation of absorbance intensity. The results show the strongest absorbance in the UV region of 250–400 nm increase with layer

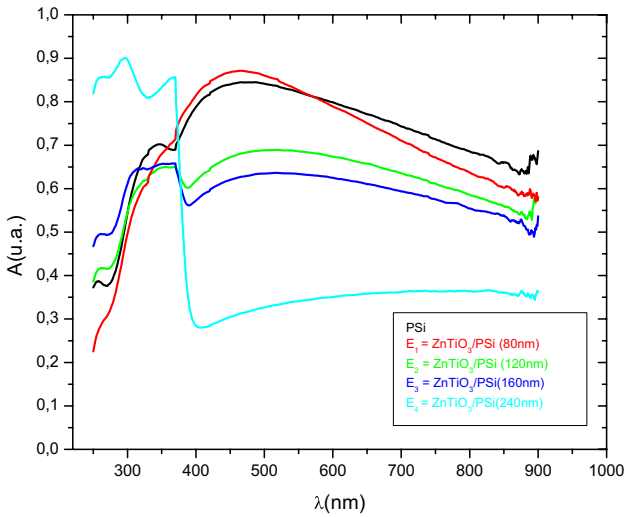

Fig. 3 UV-Vis spectra of $ZnTiO_3$ nanostructures with different thickness grown on PSi substrate

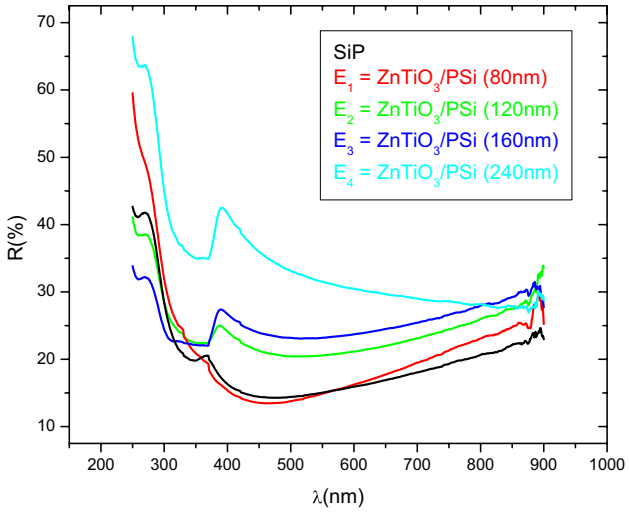

Fig. 4 Reflectivity of $ZnTiO_3$ nanostructures with different thickness grown on PSi substrate

thickness of $ZnTiO_3$. Figure 3 shows the absorption intensity increase of E_1, compared to porous silicon and the other samples. The enhanced absorption of $ZnTiO_3$ due to the Surface Plasmon Resonance (SPR) of the free electrons and $ZnTiO_3$ incorporated in pores.

Figure 3 shows the absorption intensity in visible region decrease with layer thickness of $ZnTiO_3$. It is because the layer become thick, getting larger and smoother, causing a reduction in the absorption optical.

The sample E_4 has high UV absorbance, which indicates this sample has synergistically enhanced UV absorption behavior. This is very beneficial for enhanced anti-UV aging performance. These conclusions are consistent with the statistical results as shown in Fig. 4.

Figure 4 shows UV–vis reflectance spectra of PS (black line), E_1 (red line), E_2 (green line), E_3 (blue line) and E_4 (light blueline) structures for the wavelength range of 250 nm–900 nm. The reflectivity of the porous silicon surface without $ZnTiO_3$ was around 14.3% and decreased to around 13.4% after layer of $ZnTiO_3$ deposed on porous silicon at around 450 nm. This is due to the formation of needle-like structures that result in enhanced light trapping. The decreased reflectivity results in significant increase of absorbance in E_1. It can be observed from the spectra that the optical reflectance spectra of $nZnTiO_3$/PS increased significantly with thickness layer. The increased reflectance results in significant decrease of absorbance in E_2, E_3 and E_4.

3.3 HRTEM Study

The microstructural information of the samples was obtained using transmission electron microscopy (TEM). Figure 5a shows a TEM image of $ZnTiO_3$ grown on Si (a, c) (A) and PS (b) (B). As can be seen, the $ZnTiO_3$ was fully crystalline at the nanoscale and the formation of irregular spherical shaped. The TEM images (Fig. 5) suggest that the submicrosized particles of A and B are both crystalline with no apparent defects and dislocations. The average diameters of the smallest visible isolated particle/crystallite agglomerate were found to range between 100 nm and 120 nm for A and the particles B with the size of about 80 nm. These results are in excellent agreement with the experimental of values obtained from XRD.

Figure 6 shows surface morphology of $ZnTiO_3$ particle. Note that the microstructure of B becomes a sponge. This last composed of nanopores. On the other hand, the structure is smooth and lacks pores for A. These results are in parallel with UV-Vis results. The porous structure of $ZnTiO_3$ influences the increases light absorption (UV-Vis) compared to A (Fig. 2).

The HRTEM image of the sample is presented in Fig. 7. The distance between the adjacent lattice fringes is 0.38 and 0.1 nm for A and B, which can be assigned to the interplanar distance of the hexagonal phases of A and B. Compared with compound A, the crystallinity of B is better. Comprehensively, the results confirmed that the $ZnTiO_3$ layers were successfully prepared at annealing temperatures at 700 °C.

4 Conclusion

In summary, we have synthesized nanoscale $ZnTiO_3$ on PS and Si. The dependence of the structural and optical properties of these nanostructures on the different substrates was investigated systematically. The

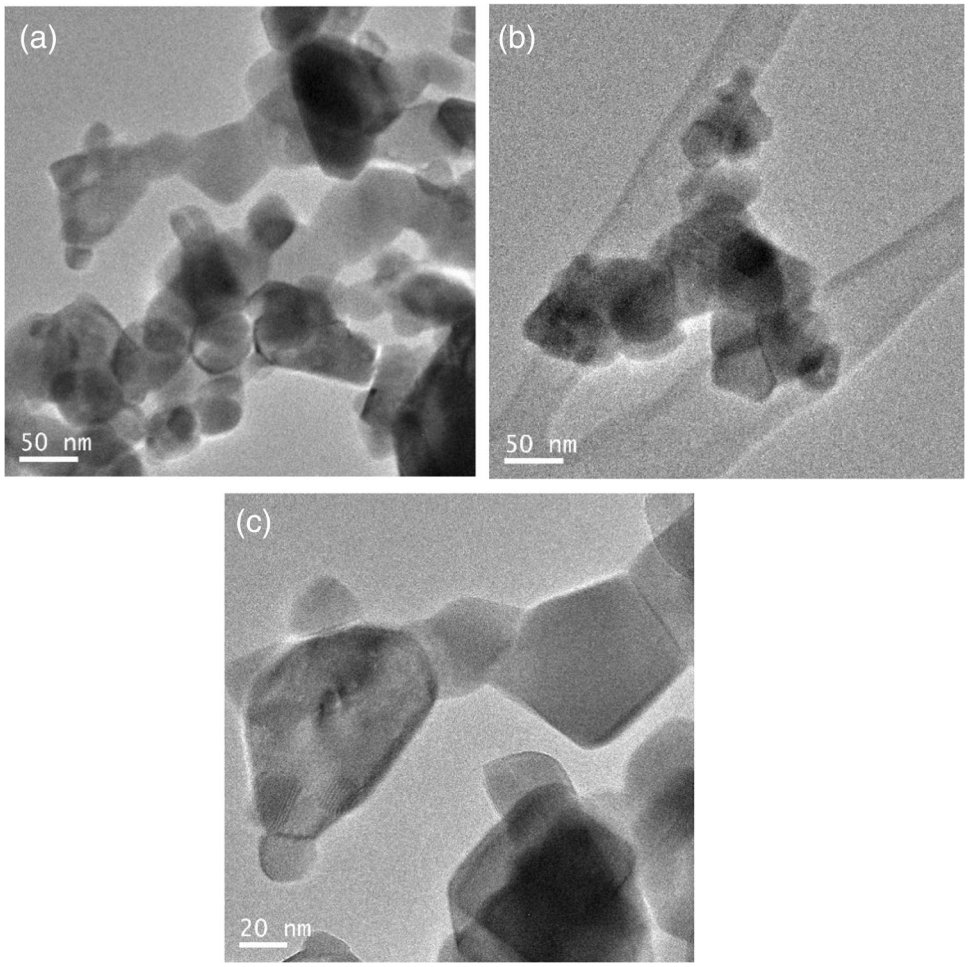

Fig. 5 TEM image of the $ZnTiO_3$ grown on Si (**a**, **c**) and PS (**b**)

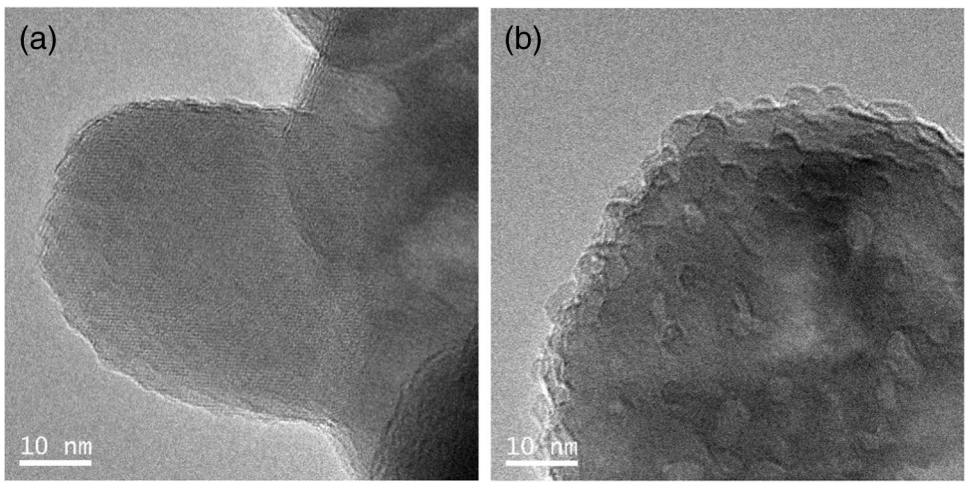

Fig. 6 TEM image of the surface $ZnTiO_3$ grown on Si (**a**) and PS (**b**)

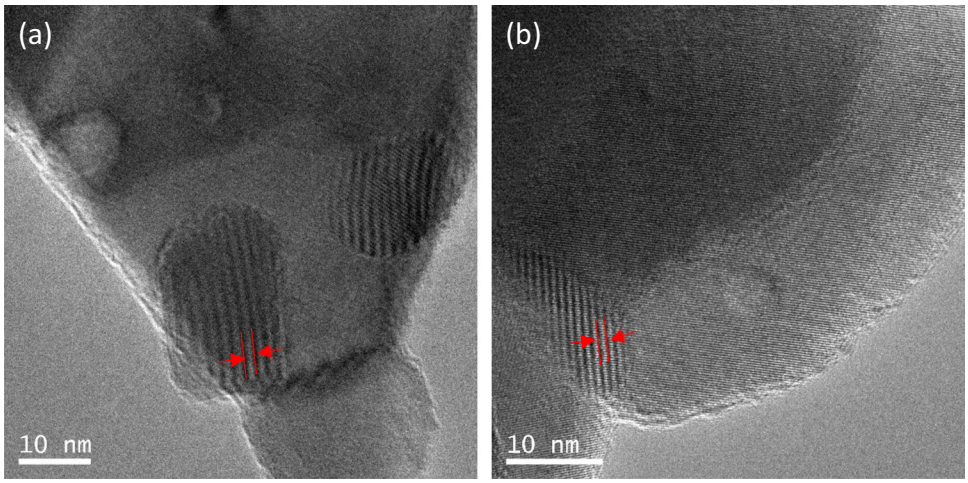

Fig. 7 HRTEM images of $ZnTiO_3$ grown on Si (**a**) and PS (**b**)

nanostructures were polycrystalline in nature, (410) plane was the preferred orientation, and showed decreasing crystal grain size with porous silicon substrates. A strongest UV-Vis absorption intensity for $ZnTiO_3$ nanoscale have been obtained on PS substrate compared to $ZnTiO_3$ as grown on Si substrate. This is due to the capillary effect and its high specific surface area of PS. With HRTEM, We compared the structure and morphology of $ZnTiO_3$ nanostructures grown on porous silicon and silicon substrate. The average diameter and the distance between the adjacent lattice fringes of these $ZnTiO_3$ on porous silicon decreased from 120 to 80 nm and from 0.38 to 0.1 nm, respectively.

Acknowledgements The authors would like to acknowledge financial support from the Research and Technology Centre of Energy (CRTEn).

Authors' Contributions Marouan khalifa and Khadija hammedi wrote the main manuscript. Hatem Ezzaouia and Chaker Bouzidi prepared figures. All authors reviewed the manuscript.

Funding This complete work has been fnancial supported by Research and Technology Centre of Energy (CRTEn).

Data Availability Not applicable.

Declarations

Ethics Approval Not applicable.

Consent to Participate Not applicable.

Consent for Publication The Author hereby consents to the publication of the work in the "Silicon" journal.

Competing Interests The author declares that there is no confict of interest in the printing of this manuscript.

References

1. Fatima H, Azhar MR, Khiadani M, Zhong Y, Wang W, Su C, Shao Z (2022) Prussian blue-conjugated ZnO nanoparticles for near-infrared light-responsive photocatalysis. Materials Today Energy 23:100895. https://doi.org/10.1016/j.mtener.2021.100895
2. Özdemir AO, Caglar B, Çubuk O, Coldur F, Kuzucu M, Guner EK, Doğan B, Caglar S, Özdokur KV (2022) Facile synthesis of TiO_2-coated cotton fabric and its versatile applications in photocatalysis, pH sensor and antibacterial activities. Mater Chem Phys 287:126342. https://doi.org/10.1016/j.matchemphys.2022.126342
3. Li Y, Min F, Wang R, Siwei W, Tan X (2022) Efficient removal TC by Zn@SnO2/PI via the synergy of adsorption and photocatalysis under visible light. Chem Eng J 444:136567. https://doi.org/10.1016/j.cej.2022.136567
4. Dhatarwal P, Sengwa RJ (2021) Poly(vinyl pyrrolidone) matrix and SiO2, Al2O3, SnO2, ZnO, and TiO2 nanofillers comprise biodegradable nanocomposites of controllable optical properties for optoelectronic application. Optik 241:167215. https://doi.org/10.1016/j.ijleo.2021.167215
5. Fan W, Qiao Q, Bahrami B, Chen K, Pathak R, Mabrouk S, Tong Y, Li X, Zhang T, Jian R (2018) Comparison of performance and optoelectronic processes in ZnO and TiO2 nanorod array-based hybrid solar cells. Appl Surf Sci 456:124. https://doi.org/10.1016/j.apsusc.2018.06.097
6. Senthilkumar P, Raja S, Ramesh Babu R, Vasuki G (2022) Enhanced electrical and optoelectronic properties of W doped SnO2 thin films. Opt Mater 126:112234. https://doi.org/10.1016/j.optmat.2022.112234
7. Bakour A, Saadoune A, Bouchama I, Dhiabi F, Boudour S, Saeed MA (2022) Effect and optimization of ZnO layer on the performance of GaInP/GaAs tandem solar cell. Micro Nanostructures 168:207294. https://doi.org/10.1016/j.micrna.2022.207294
8. Al-She'irey AY, Balouch A, Mawarnis ER, Roza L, Rahman MYA, Abdullah, Mahar AM (2022) Effect of ZnO seed layer annealing temperature on the growth of ZnO nanorods and its catalytic application. Opt Mater 131:112652. https://doi.org/10.1016/j.optmat.2022.112652
9. Lu T s, Lv J, Wang C (2022) Hydrogenation process enhances radiation-stability of ZnO, Ga_2O_3 and TiO_2. J Alloys Compd 897:163135. https://doi.org/10.1016/j.jallcom.2021.163135

10. Enebe GC, Lukong VT, Mouchou RT, Ukoba KO, Jen T-C (2022) Optimizing nanostructured TiO2/Cu2O pn heterojunction solar cells using SCAPS for fourth industrial revolution. Mater Today: Proc 62:S145. https://doi.org/10.1016/j.matpr.2022.03.485
11. Tian X, Cui X, Lai T, Ren J, Yang Z, Xiao M, Wang B, Xiao X, Wang Y (2021) Gas sensors based on TiO_2 nanostructured materials for the detection of hazardous gases: a review. Nano Mater Sci 3:390. https://doi.org/10.1016/j.nanoms.2021.05.011
12. Koley S (2021) Engineering Si doping in anatase and rutile TiO2 with oxygen vacancy for efficient optical application. Phys B Condens Matter 602:412502. https://doi.org/10.1016/j.physb.2020.412502
13. Kumar RR, Kumar KU, Haranath D (2022) Synthesis, characterization, and applications of ZnO–TiO2 nanocomposites. Nanoscale Compound Semiconductors and their Optoelectronics Applications Woodhead Publishing Series in Electronic and Optical Materials 271. https://doi.org/10.1016/B978-0-12-824062-5.00011-7
14. Jiang Q, Han Z, Qian Y, Yuan Y, Ren Y, Wang M, Cheng Z (2022) Enhanced visible-light photocatalytic performance of ZIF-8-derived ZnO/TiO2 nano-burst-tube by solvothermal system adjustment. J Water Process Eng 47:102768. https://doi.org/10.1016/j.jwpe.2022.102768
15. Thi TDN, Nguyen LH, Nguyen XH, Phung HV, Vinh THT, Van Viet P, Van Thai N, Le HN, Pham DT, Van HT, Thi LHT, Thi TDP, Le Minh T, Quang HHP, Hoang Phuong Nguyen V, Duc TT, Nguyen HM (2022) Enhanced heterogeneous photocatalytic perozone degradation of amoxicillin by ZnO modified TiO2 nanocomposites under visible light irradiation. Mater Sci Semicond Process 142:106456. https://doi.org/10.1016/j.mssp.2022.106456
16. Heng Z, Wan Y, Xia C (2022) Calcium stabilized La0.6Sr0.4Fe0.8Mn0.2O3-δ perovskite as ceramic fuel electrode for solid oxide cell. J Power Sources 537:231535. https://doi.org/10.1016/j.jpowsour.2022.231535
17. Flores-Lasluisa JX, Huerta F, Cazorla-Amorós D, Morallón E (2022) Transition metal oxides with perovskite and spinel structures for electrochemical energy production applications. Environ Res 214:113731. https://doi.org/10.1016/j.envres.2022.113731
18. Syue Y-K, Hsu K-C, Fang T-H, Lee C-I, Shih C-J (2022) Characteristics and gas sensor applications of ZnO-perovskite heterostructure. Ceram Int 48:12585. https://doi.org/10.1016/j.ceramint.2022.01.126
19. Ashiq MGB, Mahmood Q, Haq BU, Flemban TH, Kattan NA, Alshahrani T, Laref A (2022) The study of electronics, optoelectronics, thermoelectric, and mechanical properties of Zn/CdSnO3 perovskites. Mater Sci Semicond Process 137:106229. https://doi.org/10.1016/j.mssp.2021.106229
20. Feng C, Gao Q, Xiong G, Chen Y, Pan Y, Fei Z, Li Y, Yukun L, Liu C, Liu Y (2022) Defect engineering technique for the fabrication of LaCoO3 perovskite catalyst via urea treatment for total oxidation of propane. Appl Catal B Environ 304:121005. https://doi.org/10.1016/j.apcatb.2021.121005
21. Kavitha K, Sivakumar A (2022) Synthesis and characterisation of cerium doped bismuth titanate proficient UV shielding and NIR reflective reddish brown pigment by citrate auto combustion synthesis. Inorg Chem Commun 136:109162. https://doi.org/10.1016/j.inoche.2021.109162
22. Singh S, Perween S, Ranjan A (2021) Dramatic enhancement in adsorption of Congo red dye in polymer-nanoparticle composite of polyaniline-zinc titanate. J Environ Chem Eng 9:105149. https://doi.org/10.1016/j.jece.2021.105149
23. Hidehito O, Yo S, Tetsuo G (1976) Perovskite-type oxides as ethanol sensors. J Solid State Chem 17:299. https://doi.org/10.1016/0022-4596(76)90135-3
24. Tae KH, Sahn N, Dong BJ, Yoonho K (1999) Low-fired (Zn,Mg)TiO3 microwave dielectrics. J Am Ceram Soc 82:3476. https://doi.org/10.1111/j.1151-2916.1999.tb02268.x
25. Lv J, Tang M, Quan R, Chai Z (2019) Synthesis of solar heat reflective ZnTiO3 pigments with novel roof cooling effect. Ceram Int 45:15768. https://doi.org/10.1016/j.ceramint.2019.05.081
26. Tuna Ö, Simsek EB, Sarıoğlan A, Çetin YD (2020) Multifunctional and highly active zinc titanate incorporated with copper for adsorptive hot syngas desulfurization and photocatalytic dye degradation. J Taiwan Inst Chem Eng 112:388. https://doi.org/10.1016/j.jtice.2020.04.008
27. Bartram S, Slepetys RA (1961) Compound formation and crystal structure in the system ZnO-TiO2. J Am Ceram Soc 44:493. https://doi.org/10.1111/J.1151-2916.1961.TB13712.X
28. Yamaguchi O, Morimi M, Kawabata H, Shimizu K (1987) Formation and transformation of ZnTiO3. J Am Ceram Soc 70:97. https://doi.org/10.1111/j.1151-2916.1987.tb05011.x
29. Chang Y-S, Chang Y-H, Chen I-G, Chen G-J, Chai Y-L (2002) Synthesis and characterization of zinc titanate nano-crystal powders by sol–gel technique. J Cryst Growth 243:319. https://doi.org/10.1016/S0022-0248(02)01490-2
30. Chai Y-L, Chang Y-S, Chen G-J, Hsiao Y-J (2008) The effects of heat-treatment on the structure evolution and crystallinity of ZnTiO3 nano-crystals prepared by Pechini process. Mater Res Bull 43:1066. https://doi.org/10.1016/j.materresbull.2007.06.002
31. Wang C-L, Chu H-L, Ko H-H, His C-S, Li W-L, Hwang W-S, Chang K-M, Wang M-C (2015) Phase formation mechanism of the zinc titanate precursor powders prepared at various pH using a hydrothermal process. Ceram Int 41:2028. https://doi.org/10.1016/j.ceramint.2014.09.131
32. Shyh-Chi W, Jeng Y-R, Yau W-H, Kuan-Te W, Tsai C-H, Chou C-P (2012) Nanoindentation response of zinc titanate thin films deposited by co-sputtering process. Appl Surf Sci 258:6730. https://doi.org/10.1016/j.apsusc.2012.02.076
33. Gonzales LL, da Silva Hartwig M, Fassbender RU, Moreira EC, Pereira MB, Jardim PLG, Raubach CW, Moreira ML, Cava SS (2021) Properties of zinc titanates synthesized by microwave assisted hydrothermal method. Heliyon 7:e06521. https://doi.org/10.1016/j.heliyon.2021.e06521
34. Liu X (2012) Molten salt synthesis of ZnTiO3 powders with around 100 nm grain size crystalline morphology. Mater Lett 80:69. https://doi.org/10.1016/j.matlet.2012.04.048
35. Phani AR, Passacantando M, Santucci S (2007) Synthesis of nanocrystalline ZnTiO3 perovskite thin films by sol–gel process assisted by microwave irradiation. J Phys Chem Solids 68:317. https://doi.org/10.1016/j.jpcs.2006.09.010
36. Morsi RMM, Margha FH, Hamzawy EMA (2019) Preparation and electrical characterization of Zn-Titanate / borosilicate glass composites. Silicon 11:1845. https://doi.org/10.1007/s12633-018-0003-1
37. Habibi MH, Mikhak M (2012) Titania/zinc oxide nanocomposite coatings on glass or quartz substrate for photocatalytic degradation of direct blue 71. Appl Surf Sci 258:6745. https://doi.org/10.1016/j.apsusc.2012.03.042
38. Jain PK, Salim M, Kaur D (2016) Effect of phase transformation on optical and dielectric properties of pulsed laser deposited ZnTiO3 thin films. Superlattice Microst 92:308. https://doi.org/10.1016/j.spmi.2016.02.018
39. Khudiar SS, Mutlak FA-H, Nayef UM (2021) Synthesis of ZnO nanostructures by hydrothermal method deposited on porous silicon for photo-conversion application. Optik 247:167903. https://doi.org/10.1016/j.ijleo.2021.167903

40. Rahmani N, Dariani RS (2016) Effect of porous silicon buffer under different porosities on lateral overgrowth of TiO2 nanorods on silicon substrate. J Alloys Compd 681:421. https://doi.org/10.1016/j.jallcom.2016.04.234
41. Rahmani N, Dariani RS, Rajabi M (2016) A proposed mechanism for investigating the effect of porous silicon buffer layer on TiO2 nanorods growth. Appl Surf Sci 366:359. https://doi.org/10.1016/j.apsusc.2016.01.075
42. Dutta DP, Singh A, Tyagi AK (2014) Ag doped and Ag dispersed nano ZnTiO3: improved photocatalytic organic pollutant degradation under solar irradiation and antibacterial activity. J Environ Chem Eng 2:2177. https://doi.org/10.1016/j.jece.2014.09.015
43. Raveendra RS, Prashanth PA, Hari Krishna R, Bhagya NP, Sathyanarayani S, Nagabhushana BM (2017) Carbothermal synthesis and photoluminescence characteristics of pure Undoped ZnTiO3 nanocrystals. J Adv Phys Sci 2:1. https://doi.org/10.1016/j.jece.2014.09.015
44. Abdulgafour HI, Yam FK, Hassan Z, AL-Heuseen K, Jawad MJ (2011) ZnO nanocoral reef grown on porous silicon substrates without catalyst. J Alloys Compd 509:5627. https://doi.org/10.1016/j.jallcom.2011.02.100
45. Habibi MH, Mikhak M (2011) Synthesis of Nanocrystalline zinc Titanate Ecandrewsite by sol-gel: optimization of heat treatment condition for red shift sensitization. Curr Nanosci 7:603. https://doi.org/10.2174/157341311796196754
46. Habibi MH, Mikhak M, Zendehdel M, Habibi M (2012) Influence of nanostructured zinc titanate, zinc oxide or titanium dioxide thin film coated on fluorine doped tin oxide as working electrodes for dye-sensitized solar cell. Int J Electrochem Sci 76787. Web of Science Id WOS:000307980800017